

NJC

Accepted Manuscript



This is an *Accepted Manuscript*, which has been through the Royal Society of Chemistry peer review process and has been accepted for publication.

Accepted Manuscripts are published online shortly after acceptance, before technical editing, formatting and proof reading. Using this free service, authors can make their results available to the community, in citable form, before we publish the edited article. We will replace this *Accepted Manuscript* with the edited and formatted *Advance Article* as soon as it is available.

You can find more information about *Accepted Manuscripts* in the [Information for Authors](#).

Please note that technical editing may introduce minor changes to the text and/or graphics, which may alter content. The journal's standard [Terms & Conditions](#) and the [Ethical guidelines](#) still apply. In no event shall the Royal Society of Chemistry be held responsible for any errors or omissions in this *Accepted Manuscript* or any consequences arising from the use of any information it contains.

Cite this: DOI: 10.1039/c0xx00000x

www.rsc.org/xxxxxx

ARTICLE TYPE

Straw-sheaf-like terbium-based coordination polymer architectures: Microwave-assisted synthesis and their application as selective luminescent probes for heavy metal ions

Mengmeng Shi, Zeng Chenghui, Lei Wang, Zhiwen Nie, Yongxia Zhao, Shengliang Zhong*

Received (in XXX, XXX) Xth XXXXXXXXXX 20XX, Accepted Xth XXXXXXXXXX 20XX
DOI: 10.1039/b000000x

Straw-sheaf-like terbium-based coordination polymer (CP) architectures have been successfully synthesized through a simple, facile and environmentally friendly microwave heating approach on a large scale in 15 min without the assistance of any template or surfactant employing 1,2,4,5-benzenetetracarboxylic acid (H_4BTC) as the organic building block. The composition and structure of the samples were well characterized by powder X-ray diffraction (XRD), elemental analyses (EA), Fourier transform infrared (FT-IR), thermogravimetric analysis (TG), X-Ray photoelectron spectroscopy (XPS) and scanning electron microscopy (SEM). The specific surface area was determined by the Brunauer-Emmett-Teller (BET) method. The measured specific surface area of the terbium-based CP was $152.51\text{ m}^2\text{g}^{-1}$. SEM results showed that the individual straw-sheaf have a length in the range of 70-90 μm and a middle diameter in the range of 5-8 μm . A possible mechanism responsible for the formation of the straw-like sheaves hierarchical architectures was proposed. The products showed strong characteristic of green emissions under ultraviolet excitation, well corresponding to the $^5D_4 \rightarrow ^7F_J$ transitions of Tb^{3+} ions. Furthermore, it displayed highly sensitive and selective luminescence quenching to Pb^{2+} in aqueous solution.

1. Introduction

CP or metal organic framework (MOF) has recently emerged as interesting functional materials because they can be made from readily available and highly tailorable metal and ligand precursors.¹⁻³ Among the diverse CP particles, the lanthanide CPs (Ln-CPs), an important member of the CP family, have received great attention, due to their characteristic coordination preferences and unique optical and magnetic properties arising from their 4f electrons.^{4,5} Ln-CPs have attracted much attention not only because of their fascinating architectures but also for their extensive applications in high performance luminescence sensors, magnets, catalysts, and other functional materials.⁶⁻¹² Some Ln-CPs have been successfully used as luminescent probes for the detection of metal ions. For example, Yang and his co-workers reported a novel highly luminescent Ln-CP film for detection of Hg^{2+} ions.¹³ The Sun group designed a fluorescent probe for sensing Fe^{3+} ions.¹⁴ Various benzoic multicarboxylates have been employed to construct Ln-CPs. For instance, 1,4-benzene dicarboxylic acid (p- H_2BDC) with a 180 degree angle separation between the two

carboxylate groups,¹⁵ benzene-1,3,5-tricarboxylic acid (H_3BTC) with a 120 degree angle between two carboxylic groups,^{16,17} H_4BTC which has a highly centrosymmetric geometry, are all widely used as linkers of metal ions in the construction of CPs.^{18,19} In particular, H_4BTC has drawn considerable attention because of its specially outstanding inherent chemical features as follows: (a) its multicarboxylate groups with oxygen atoms acting as a hard base, are especially preferable to bond to lanthanide metal ions; (b) it has four potential carboxyl groups that may be completely or partially deprotonated and exhibit a variety of interesting coordination modes towards metal ions, which can bring unforeseen structure patterns and packing frameworks; (c) it possesses high symmetry that may be helpful for improving the coordination capability to metal ions and for enhancing the stability of CPs. These features are particularly valuable for developing functional Ln-CPs. Recently, our group has successfully prepared three-dimensional flowerlike cerium-based CP hierarchical architectures, using H_4BTC as the organic linker under solvothermal condition.²⁰ To date, with the development of nanoscience and nanotechnology, several synthetic strategies for the preparation of CP nanomaterials have been developed and a large number of CPs have been prepared based on the methods as precipitation, reverse microemulsion, hydrothermal, electrospinning.²¹⁻²⁴ In the

College of Chemistry and Chemical Engineering, Jiangxi Normal University, Nanchang 330022, China.

Electronic supplementary information (ESI) available: additional graphs.

See DOI: 10.1039/c00000000x.

past decade years, CPs were commonly synthesized under the hydro- or solvothermal conditions which usually requires relatively long reaction times (days to weeks) and high temperature, which limited the prospect of its application.

Furthermore, the fabrication of CPs with complex morphologies is still challenging. Developing facile and economical routes for the syntheses of CPs has been a challenging task for practical applications. The microwave method (MW) displays many advantages such as: fast crystallization, diverse morphology, decreasing size of crystallites. Microwave-assisted reaction can dramatically reduce the reaction time and hold promise for potentially large-scale industrial productions.^{25,26} It provides an efficient way to control particle size distribution which is very important in new applications of CPs.

Lead (Pb^{2+}) is one of the most abundant and toxic heavy metal ions. Once introduced into human's body it will cause serious harmful effects on the nervous system, immune system, reproductive system, especially infants and children. Beside, Pb^{2+} may lead to a serious threat to flora and fauna. Thus, the sensing of Pb^{2+} in the environment and biology systems is very important. There are various techniques to detect metal ions at low levels such as atomic absorption spectrometry, inductively coupled plasma mass spectrometry, and voltammetry etc.^{27,28} However, these widely-used conventional methods which can detect heavy metal sensitively and accurately often require complicated sample pre-treatment, expensive cost, expert operators and are time-consuming, not suitable for real-time test. In recent years, fluorescence probe has been widely used because of its high sensitivity, selectivity, simple application, and low cost. Much research on probes for fluorescence detection has been done in the past few decades.^{29,30} In this paper, we used H_4BTC along with a series of lanthanide salts in a mixed solution of N,N -dimethylformamide (DMF) and water to produce uniform novel straw-sheaf-like CPs on a large scale with the assistance of microwave heating in a short time. We also proposed a possible mechanism for the formation of the straw-like sheaves hierarchical architectures. So far, many fluorescent probes for Hg^{2+} , Fe^{3+} , Cu^{2+} , Cr^{3+} have been reported.³¹⁻³⁵ To the best of our knowledge, few reports have appeared on the usage of fluorescent probes for Pb^{2+} ions based on luminescence changes in aqueous solution.³⁶⁻³⁸ Furthermore, Ln-CPs nanoparticles have not been explored to detect Pb^{2+} ions in aqueous solution.

2. Experimental section

2.1 Materials and general methods

All the chemical reagents used in this experiment were of analytical grade and used without further purification.

In a typical experiment, 12 mL deionized water containing 0.1 mmol of $\text{Tb}(\text{NO}_3)_3 \cdot 6\text{H}_2\text{O}$ and 3 mL of DMF solution containing 0.1 mmol of H_4BTC were poured into a 100 mL round bottom flask under vigorous stirring. The mixture was stirred for 15 min at room temperature and then got heated in a microwave furnace for 15 min. The microwave power and frequency were set at 80 W and 2.45 GHz, respectively. After reaction, the temperature of the reaction mixture was detected to be about 100 °C. In our experiments, the microwave oven we used is a modified household microwave oven equipped with a refluxing apparatus.

After being irradiated for 15 min under an air atmosphere, the samples were cooled to room temperature naturally and the precipitates were separated by centrifugation and washed several times with deionized water and ethanol. Finally the products were dried at 60 °C in a vacuum oven for further characterization.

2.2 Characterization

XRD analysis was carried out by using a Rigaku X-ray diffractometer with $\text{Cu-K}\alpha$ radiation ($\lambda = 1.54178 \text{ \AA}$). The morphology of the samples was inspected by using a scanning electron microscope equipped with an energy dispersive X-ray spectrum (EDX), (Hitachi, S-3400N). Elemental analyses (C, H and O) were performed on an EA3000 elemental analyzer. Infrared (IR) spectra were measured on a Perkin-Elmer SP one FT-IR spectrometer in a KBr pellet, scanning from 4000 to 400 cm^{-1} at room temperature. TG analysis was carried out with a heating rate of 10 °C min^{-1} in air from room temperature to 1000 °C by using a Diamond TG/DTA simultaneous thermal analyzer. X-ray photoelectron spectroscopy measurement (XPS) was performed on a Thermo VG Scientific, ESCALAB 250 equipped with monochromatic $\text{Al K}\alpha$ as radiation source. The nitrogen physisorption isotherms were measured at liquid nitrogen temperature (77 K) using a BELSORP-mini II apparatus. The sample was degassed at 100 °C under vacuum. Photoluminescence (PL) excitation, emission spectra and lifetime were recorded on an (Edinburgh Instruments, England) FLS 980 at room temperature.

3. Results and discussion

3.1 structure, composition, properties and morphology characterization of the typical product

The chemical composition and crystal structure of the typical product were firstly determined by XRD measurements. As shown in Fig. 1, it indicates that it is amorphous and not crystalline. The specific surface area was determined using N_2 adsorption/desorption analysis. The N_2 adsorption/desorption isotherms are shown in Fig. 2. The BET surface area and total pore volume of the terbium-based CP are 152.51 m^2g^{-1} and 1.0515 cm^3g^{-1} , respectively. According to the IUPAC classification, the obtained isotherm can be recognized as a type IV N_2 adsorption/desorption isotherm.

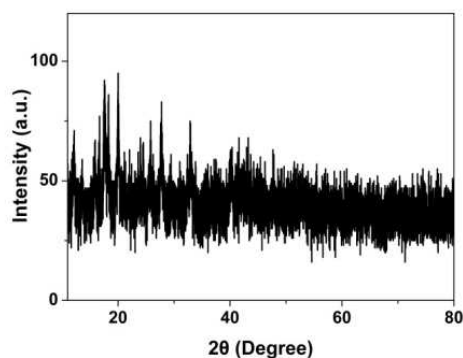


Fig. 1 XRD pattern of the typical product.

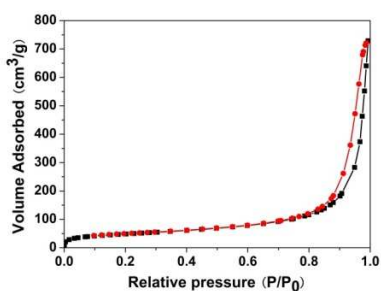


Fig. 2 Nitrogen adsorption–desorption isotherms of the typical product.

The morphology and structure of the typical products were examined by SEM. As can be seen in Fig. 3a, b, there are a large scale of products which look like straw-sheaves with two bundles and consist of a bundle of outspread nanowires which are closely bonded to each other in the middle. Careful observations (Fig. 3c, d) reveal that the individual straw-sheaf has a length in the range of 70–90 μm and a middle diameter in the range of 5–8 μm . The morphology is similar to those reported in the literature.^{17,39–42} The vast majority of the reported products are inorganic and synthesized through a hydrothermal route which is time- and energy-consuming and whose experimental process is difficult to handle. You and his co-workers have prepared CP Pr(1,3,5-BTC)(H₂O)₆ straw-sheaf-like architectures through one-step precipitation in solution phase.¹⁷ By comparison, our products show a high degree of uniformity and are much bigger than any other reported products.

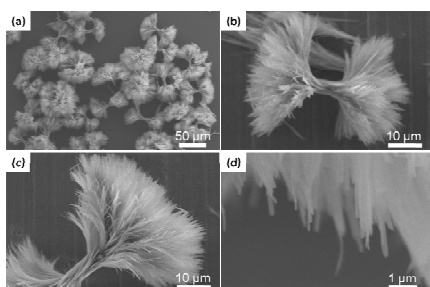


Fig. 3 SEM images of the as-prepared straw-sheaf-like typical product.

As we all know, lanthanide atoms have ionic radii which are close to each other and change gradually. As a result, the chemical and physical properties change correspondingly. Some other Ln-H₄BTC (Ln = La, Ce, Pr, Nd, Sm, Eu, Gd, Dy, Ho, Er, Tm, Yb, Lu) CPs were also prepared under the same reaction conditions (Table S1, Fig. S1, Fig. S2 ESI†). The whole growth regions can be classified into two distinct groups, La–Nd, Tm, Yb, and Sm–Lu (except for Tm and Yb). All the products take the shape of sheaf-like hierarchical architectures. Among them, the morphologies of the Ln-H₄BTC (Ln = La–Nd, Tm, Yb) are mainly composed of rod-sheaf-like structures. And the others are straw-sheaf-like. Based on the above results, it can be concluded that although the synthetic conditions are identical for all rare earth ions, the morphology of Ln-H₄BTC microstructures are different. We can find out that rare earth ions with bigger ionic radii generally show rod-sheaf-like morphologies, the smaller ones show straw-sheaf-like. As to Tm and Yb complex, the difference may be attributed to electronic configuration, because

Tm³⁺ and Yb³⁺ have nearly full-filled electrons in the f orbital. The formation process of hierarchical architectures is a complex one. These differences can be simply ascribed to the well known effect of lanthanide contraction and the anisotropic growth process.^{20,43} The dimensionalities of these CPs are dependent on the nature of the lanthanide cations.

To demonstrate that the H₄BTC molecules had been bonded onto the CPs, the FT-IR spectra were measured (Fig. S3, ESI†). From the standard FT-IR spectrum, the broad band at 3371 cm⁻¹ shows that the complex contains water molecules. Moreover, the spectrum shows two peaks at 1592 cm⁻¹ and 1395 cm⁻¹, corresponding to the asymmetric and symmetric stretching vibration of carboxyl, respectively.⁴⁴ The peak at 1625 cm⁻¹ implying that the carboxyls of H₄BTC have partially coordinated with Tb³⁺ by acid radicals.⁴⁵ The red shift from 1700 cm⁻¹ of H₄BTC may be caused by strong hydrogen bonding between uncoordinated water molecule and the protonated carboxyl group, indicating the formation of H₄BTC complex.

To determine the composition of the typical product, the chemical composition of the straw-sheaves was further investigated with EDX (Fig. S4, ESI†) and elemental analysis. The result confirms that the sample is made of Tb, C, O and H. The atomic percent of C, O and Tb is 45.45, 50.76 and 3.76% from EDX spectrum. Elemental analysis shows that the contents of C, O and H are 22.673, 30.877 and 2.627%, respectively. XPS was employed to characterize the chemical states of Tb in the deposited typical products. As shown in Fig. 4. The peaks of Tb, C and O are found. The XPS spectrum of Tb shows two binding energy peaks in the 3d region at 1242.88 and 1277.88 eV (Fig. 4b), in addition to the 4d region at 151.08 eV, which can be assigned to the Tb(III) species.⁴⁶ The TG curve (Fig. 5) taken in air exhibits two major stages of rapid weight loss in the temperature range from 80 to 550 °C. The first weight loss stage before 280 °C can be ascribed to the release of the physically absorbed and structured water molecules.⁴⁷ The second weight loss from 280 to 550 °C is due to the burnout of the organic molecules. The decomposition of ligands completes above 550 °C and terbium oxide (Tb₄O₇) is formed. (Fig. S5, ESI†)

The weight loss in the two stages is measured to be 17.93% and 43.84%, respectively. This result is basically in agreement with the theoretical weight loss of the five water molecules (18.00%) and the organic ligand (44.60%) of assumed structure Tb(HBTC)(H₂O)₅. On the basis of the above consideration, we can infer that the possible molecular formula of the typical product is Tb(HBTC)(H₂O)₅.

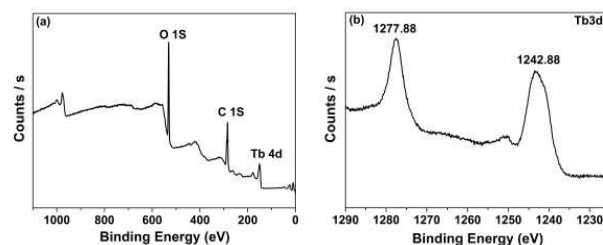


Fig. 4 XPS spectra of the typical product: (a) the survey spectrum; (b) XPS Tb 3d spectrum.

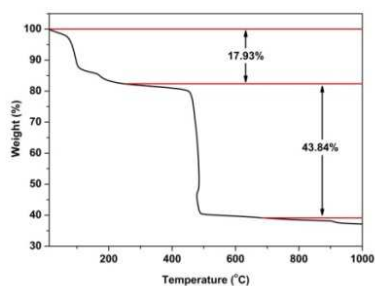


Fig. 5 TG curve of the typical product.

Lanthanide-containing CPs often exhibit intense luminescence and herewith they are particularly interesting for luminescent materials. The photoluminescence properties were investigated in detail at room temperature. The PL spectra of the Tb(HBTC)(H₂O)₅ suspension of the 4 mg sample dispersed in 20 mL H₂O are shown in Fig. 6. The excitation spectrum is shown in Fig. 6a. It can be seen from it that the complex has strong absorption at 302 nm. The emission spectrum of Tb(HBTC)(H₂O)₅ is obtained under the excitation of 302 nm. The emission spectrum is shown in Fig. 6b, which exhibits characteristic of terbium(III) emission bands resulting from the ⁵D₄→⁷F_J (J = 6, 5, 4 and 3) transitions, with 544 nm being the most strongest. The as-synthesized sample was dispersed in aqueous solution containing various metal ions for the luminescence studies. The experimental details of luminescence measurement of Tb(HBTC)(H₂O)₅ in the presence of various metal ions are as follows: (i) the powder of Tb(HBTC)(H₂O)₅ (0.2 mg) was introduced into 1 mL H₂O; (ii) the resultant suspension was treated by ultrasonic for 30 min to make the particles of Tb(HBTC)(H₂O)₅ well dispersed in H₂O; (iii) 4 mL 1×10⁻³ M aqueous solution of MCl_x (M = Ba²⁺, Cd²⁺, Co²⁺, Cr³⁺, Cu²⁺, Mn²⁺, Ca²⁺, Zn²⁺, Ni²⁺, Hg²⁺, Pb²⁺, except Hg(NO₃)₂) was used as the source of Hg²⁺ was added to the suspension of Tb(HBTC)(H₂O)₅ under continuous stirring; (iv) the mixtures were stirred for 1 hour.

Then the emission spectra were measured and compared in Fig. 7. As shown in Fig. 7, the luminescence intensity shows the quenching effect for all metal ions. Among the metal ions studied, Ba²⁺, Cr³⁺, Cu²⁺, Ca²⁺, Zn²⁺, Ni²⁺ ions have no apparent effect on the luminescence intensity, whereas the other metal ions produce varying degrees of quenching of the luminescence intensity. The quenching effects of Hg²⁺ and Pb²⁺ are very pronounced, especially for Pb²⁺ ions. The PL spectra of the Pb²⁺ ion-containing suspension at different concentrations are shown in Fig. 8. The strong green emission of the Tb(HBTC)(H₂O)₅ suspension under 254 nm laboratory UV light was completely disappeared after the addition of Pb²⁺ ions as shown in the insert in Fig. 8. In comparison with main group metal cations and transition metal cations, Pb (II) possesses a large radius, variable coordination numbers and diverse coordination geometries. Particularly, Pb²⁺ with a closed-shell electron configuration of 6s² has the strongest quenching effect. The high sensitivity has allowed us to easily identify the existence of a small amount of Pb²⁺ ions in aqueous solution, which could be used in potential application in the field of monitoring heavy metal ions. The luminescent quenching effect of Pb²⁺ on Tb(HBTC)(H₂O)₅ has been further examined by luminescence lifetime studies of Tb³⁺.

The luminescence lifetime (detected at 544 nm for the ⁵D₄→⁷F₅ transition) of the complex decreases from 980.44 μs to 864.06 μs upon treatment with the Pb²⁺ 10⁻³ M aqueous solution (Fig. S6, ESI†).

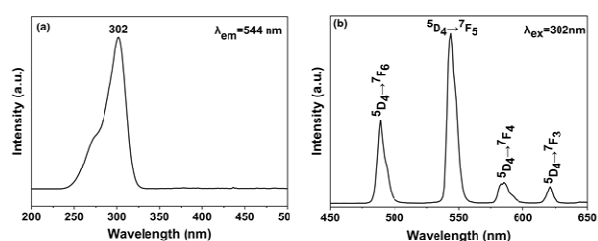


Fig. 6 Excitation (a) and emission (b) spectra of Tb(HBTC)(H₂O)₅ product.

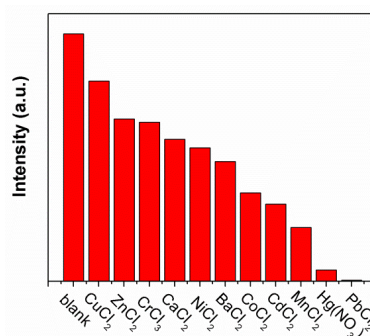


Fig. 7 Comparison of the ⁵D₄→⁷F₅ luminescence intensity of Tb(HBTC)(H₂O)₅ in different metal ion aqueous solutions.

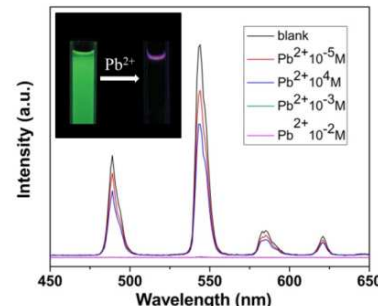


Fig. 8 The PL spectra of Tb(HBTC)(H₂O)₅ in PbCl₂ aqueous solution at different concentrations (excited at 302 nm). The inset shows the luminescence change after the addition of Pb²⁺ ions in the Tb(HBTC)(H₂O)₅ suspension under UV light.

There are many methods have been developed to detect Pb²⁺. For example, Mancin et al prepared dansyl doped silica nanoparticles and they were used to detect Pb²⁺ by fluorescence quenching. However, their experiments were complex and required delicate synthetic procedures. A residual 60% fluorescence was still detected even at very high Pb²⁺ concentrations after the addition of lead ions to buffered solutions. Even in the case of their improved systems, the residual fluorescence was still 30%.⁴⁸ Rica et al used Pb²⁺-binding peptide to develop an electrochemical impedance sensor where the Pb²⁺-binding peptide molecules physisorbed on nanotubes could detect Pb²⁺ as low as 0.01 nM. However, their detection process is sophisticated and took a very long time to finish the incubation process. Furthermore, Pb²⁺ cannot be quantified when concentrations are

higher than 1 nM due to a saturation of the binding sites on the nanotube sensor.⁴⁹ Lu's group developed a label-free colorimetric sensor based on the Pb^{2+} -dependent DNAzyme and AuNPs for Pb^{2+} with nanomolar detection limit. However, it is notable that the stability of gold colloids might be affected by various factors, such as solvent, stabilizer, surfactant, pH etc.⁵⁰ Compared with the reported methods, the method we used to detect Pb^{2+} has many advantages such as low cost, rapid analysis, and high sensitivity.

Recently, more and more researchers focused on the CPs for the applications in the area of sensing. Usually, the change of fluorescence intensity is majorly caused by energy migration, electron transfer, or other interactions between CPs and the analyte.^{33,34} In our work, we speculate that the luminescence quenching mechanism might be similar to that observed in the reported literature.^{31,32} The luminescence quenching might be caused by the addition of Pb^{2+} ions that weakened the bonds between the metallic sites and the organic ligands. When Pb^{2+} incorporate into the CP, the oxygen in the CP donates its lone-pair of electrons to the Pb^{2+} cation, forming an electron-deficient region nearby, which can receive electrons. The CP becomes an excellent electron donor upon excitation by light. As a result, the energy migration or electron transfer from the organic ligands (H_4BTC) to the metallic sites (Tb^{3+}) may be cut down, resulting in quenching of luminescence. In summary, $\text{Tb}(\text{HBTC})(\text{H}_2\text{O})_5$ demonstrates high selectivity and sensitivity for the determination of heavy metal ions, especially Pb^{2+} ions, which has potential application in the field of monitoring heavy metal ions.

3.2 Influences of Different Reaction Parameters and Possible Formation Mechanism of the $\text{Tb}(\text{HBTC})(\text{H}_2\text{O})_5$ Straw-sheaves

In general, the reaction environment has a great influence on the morphology of the hierarchical architectures of the final products. In the present system, controlled experiments were carefully performed. The molar ratio of reactants and the reaction time were altered while the other reaction conditions were kept constant. Firstly, we investigated the molar ratio of H_4BTC to Tb^{3+} . To obtain a better understanding of this effect, a series of experiments were carried out with different molar ratios of H_4BTC to $\text{Tb}(\text{NO}_3)_3 \cdot 6\text{H}_2\text{O}$, as shown in Fig. 9. When the molar ratio of H_4BTC to Tb^{3+} was 2, uniform hierarchical straw-sheaf-like architectures made of abundant nanowires with very high density were obtained on a large scale (Fig. 9a-c). The length of the products was in the range of 40–60 μm . Interestingly, when the molar ratio increased to 3, a large quantity of sheaflike structures comprising abundant nanobelts, instead of nanowires, were obtained (Fig. 9d-f), while the overall length was still ranging from 40 to 60 micrometres. Careful observations of the typical structure (Fig. 9f) indicate that the hierarchical architecture nanobelts have width of 400–800 nm, thickness of 50–90 nm, respectively.

To understand the detailed formation process of the $\text{Tb}(\text{HBTC})(\text{H}_2\text{O})_5$ hierarchical architectures, time-dependent experiments were carried out. Fig. 10 shows the SEM images of the products obtained from the same system at time intervals of 7, 9, 11 and 20 min whereby the other reaction parameters were kept unchanged. When the reaction time was shorter than 7 min, no precipitate was obtained. As the reaction time reached to 7

min, lots of nanospheres and straw-sheaf-like nanostructures were produced, as shown in Fig 10a, b. A close observation indicates that the typical straw-sheaf-like structures are in the range of 60–80 μm , and the nanospheres are with a diameter of about 200–400 nm. With prolonging the reaction time to 9 min, a large quantity of small straw-like structures comprising several nanowires and straw-sheaf-like nanostructures were obtained. After a prolonging of the reaction time to 11 min, the straw-like nanowires almost disappeared and nearly 100% yield straw-sheaf-like nanostructures were obtained. Finally, with the reaction time up to 20 min, straw-sheaf-like architectures were still preserved.

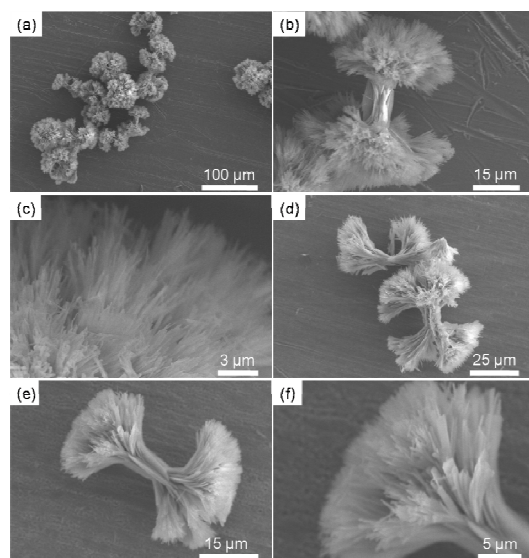


Fig. 9 SEM images of products prepared with various molar ratio of H_4BTC to Tb^{3+} : (a-c) 2 : 1; (d-f) 3 : 1.

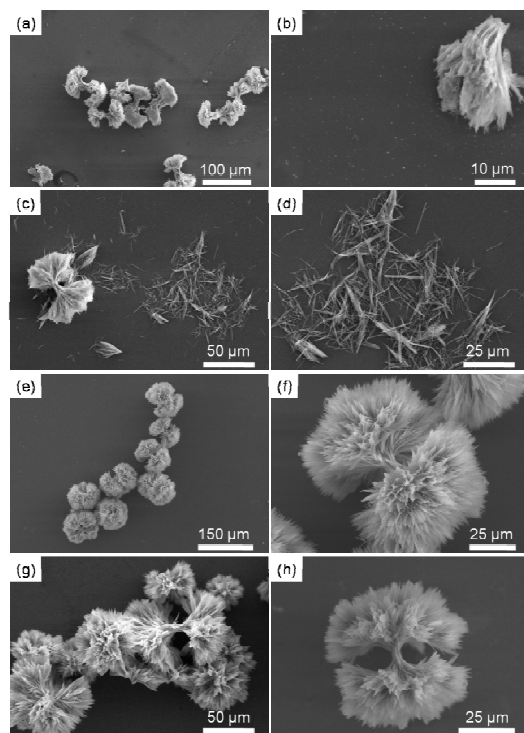
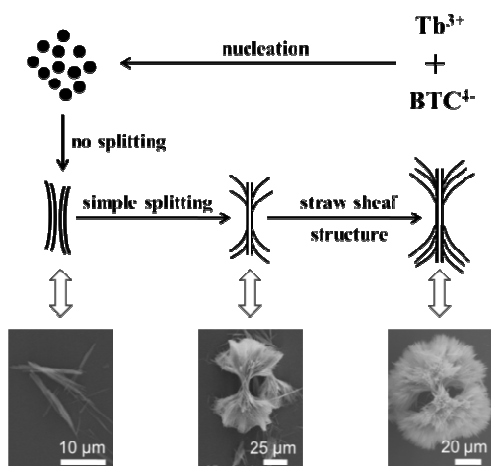


Fig. 10 SEM images of products prepared after different reaction time: (a-b) 7 min; (c-d) 9 min; (e-f) 11 min; (g-h) 20 min.



Scheme 1 A schematic of the growth process for the $\text{Tb}(\text{HBTC})(\text{H}_2\text{O})_5$ hierarchical architectures.

On the basis of the above results and analysis, the straw-sheaf-like architectures may grow according to the crystal-splitting theory proposed by the literature.^{43,51} Generally, the growth process of crystals can be classified into two steps: an initial nucleating stage and a crystal growth stage. Our experiments indicate that the nucleation and growth of the $\text{Tb}(\text{HBTC})(\text{H}_2\text{O})_5$ take place in a very short time. In the following growth process, the nuclei tend to diffuse and aggregates to form nanowires under the effects of the crystal structure and external conditions. At the same time, branches are developed on the nanowires stems, leading to the splitting. As the reaction time increasing, the branches further split into the next generation of branches, which leads to the morphology of the product transferred to micro straw-sheaf-like. The possible growth process of the straw-sheaf-like structure is summarized in Scheme 1.

4. Conclusion

$\text{Tb}(\text{HBTC})(\text{H}_2\text{O})_5$ straw-like sheaves were successfully synthesized using a mild and fast microwave-assisted method in 15 min. The formation of these complex nanostructures is supposed to be a fractal splitting growth mechanism. Moreover, the present method is simple, reliable, high-yielding, relatively green and can be further developed for the preparation of more rare earth CPs with hierarchical micro/nanostructures. We have found that the $\text{Tb}(\text{HBTC})(\text{H}_2\text{O})_5$ exhibits a remarkable quenching effect in the luminescence emission of Tb^{3+} upon the introduction of the Pb^{2+} ion. This research can be considered as a work that is devoted to the potential applications of lanthanide-CPs. Further study is needed to be focused on the function of the luminescent lanthanide-CPs to enhance their recognition sensitivity and selectivity.

Acknowledgements

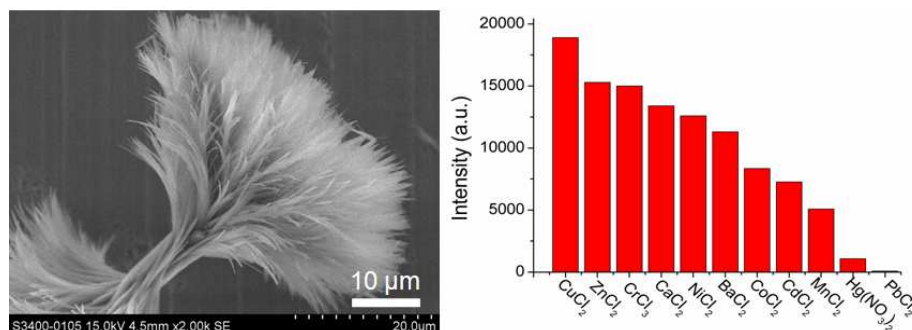
This study was funded by the National Natural Science Foundation of China (Nos. 21201089, 21261010, 61201104), Jiangxi Provincial Education Department (No. KJLD13021) and Jiangxi Provincial Department of Science and Technology (No. 20144BCB23039).

Notes and references

- J. Della Rocca, D. Liu and W. Lin, *Acc. Chem. Res.*, 2011, 44, 957.
- A. M. Spokoiny, D. Kim, A. Sumrein and C. A. Mirkin, *Chem. Soc. Rev.*, 2009, 38, 1218.
- H. R. Moon, D.-W. Lim and M. P. Suh, *Chem. Soc. Rev.*, 2013, 42, 1807.
- J. Rocha, L. D. Carlos, F. A. A. Paz and D. Ananias, *Chem. Soc. Rev.*, 2011, 40, 926.
- M. D. Allendorf, C. A. Bauer, R. K. Bhakta and R. J. T. Houk, *Chem. Soc. Rev.*, 2009, 38, 1330.
- H. Guo, Y. Zhu, S. Qiu, J. A. Lercher and H. Zhang, *Adv. Mater.*, 2010, 22, 4190.
- A. Datcu, N. Roques, V. Jubera, I. Imaz, D. Maspoch, J.-P. Sutter, C. Rovira and J. Veciana, *Chem.-Eur. J.*, 2011, 17, 3644.
- P. Wu, J. Wang, Y. Li, C. He, Z. Xie and C. Duan, *Adv. Funct. Mater.*, 2011, 21, 2788.
- K. A. White, D. A. Chengelis, K. A. Gogick, J. Stehman, N. L. Rosi and S. Petoud, *J. Am. Chem. Soc.*, 2009, 131, 18069.
- B. Chen, S. Xiang and G. Qian, *Acc. Chem. Res.*, 2010, 43, 1115.
- Z. Liu, W. He and Z. Guo, *Chem. Soc. Rev.*, 2013, 42, 1568.
- J. Luo, H. Xu, Y. Liu, Y. Zhao, L. L. Daemen, C. Brown, T. V. Timofeeva, S. Ma and H.-C. Zhou, *J. Am. Chem. Soc.*, 2008, 130, 9626.
- Y.-M. Zhu, C.-H. Zeng, T.-S. Chu, H.-M. Wang, Y.-Y. Yang, Y.-X. Tong, C.-Y. Su and W.-T. Wong, *J. Mater. Chem. A*, 2013, 1, 11312.
- M. Zheng, H. Tan, Z. Xie, L. Zhang, X. Jing and Z. Sun, *ACS Appl. Mater. Interfaces*, 2013, 5, 1078.
- S. S. Nagarkar, R. Das, P. Poddar and S. K. Ghosh, *Inorg. Chem.*, 2012, 51, 8317.
- K. Liu, H. You, Y. Zheng, G. Jia, Y. Song, Y. Huang, M. Yang, J. Jia, N. Guo and H. Zhang, *J. Mater. Chem.*, 2010, 20, 3272.
- K. Liu, Y. Zheng, G. Jia, M. Yang, Y. Huang and H. You, *CrystEngComm*, 2011, 13, 452.
- K.-L. Hou, F.-Y. Bai, Y.-H. Xing, J.-L. Wang and Z. Shi, *CrystEngComm*, 2011, 13, 3884.
- J.-L. Wang, K.-L. Hou, F.-Y. Bai, Y.-H. Xing and Z. Shi, *Struct. Chem.*, 2012, 23, 275.
- S. Zhong, M. Wang, L. Wang, Y. Li, H. M. Noh and J. H. Jeong, *CrystEngComm*, 2014, 16, 231.
- X. Sun, S. Dong and E. Wang, *J. Am. Chem. Soc.*, 2005, 127, 13102.
- K. M. L. Taylor, W. J. Rieter and W. Lin, *J. Am. Chem. Soc.*, 2008, 130, 14358.
- K. M. L. Taylor, A. Jin and W. Lin, *Angew. Chem. Int. Ed.*, 2008, 47, 7722.
- L. Xu, H. Song, B. Dong, Y. Wang, X. Bai, G. Wang and Q. Liu, *The J. Phys. Chem. C*, 2009, 113, 9609.
- K.-W. Wang, Y.-J. Zhu, F. Chen, G.-F. Cheng and Y.-H. Huang, *Mater. Lett.*, 2011, 65, 2361.
- D. Zhao, L. Wang, Y. Li, L. Zhang, Y. Lv and S. Zhong, *Inorg. Chem. Commun.*, 2012, 20, 97.
- H. N. Kim, W. X. Ren, J. S. Kim and J. Yoon, *Chem. Soc. Rev.*, 2012, 41, 3210.
- V. Arancibia, E. Nagles and S. Cornejo, *Talanta*, 2009, 80, 184.
- X. Li, X. Gao, W. Shi and H. Ma, *Chem. Rev.*, 2014, 114, 590.
- K. P. Carter, A. M. Young and A. E. Palmer, *Chem. Rev.*, 2014, 114, 4564.
- Z. Hao, X. Song, M. Zhu, X. Meng, S. Zhao, S. Su, W. Yang, S. Song and H. Zhang, *J. Mater. Chem. A*, 2013, 1, 11043.
- D. Cai, H. Guo, L. Wen and C. Liu, *CrystEngComm*, 2013, 15, 6702.
- Z. Xiang, C. Fang, S. Leng and D. Cao, *J. Mater. Chem. A*, 2014, 2, 7662.
- L. Hao, H. Song, Y. Su and Y. Lv, *Analyst*, 2014, 139, 764.
- H.-M. Wang, Y.-Y. Yang, C.-H. Zeng, T.-S. Chu, Y.-M. Zhu and S. W. Ng, *Photochem. Photobiol. Sci.*, 2013, 12, 1700.
- Y.-W. Lin, C.-W. Liu and H.-T. Chang, *Talanta*, 2011, 84, 324.
- J. Liu, K. Wu, S. Li, T. Song, Y. Han and X. Li, *Dalton Trans.*, 2013, 42, 3854.
- S. K. Saha, K. R. Ghosh, W. Hao, Z. Y. Wang, J. Ma, Y. Chiniforooshan and W. J. Bock, *J. Mater. Chem. A*, 2014, 2, 5024.

- 39 R. Jin, Y. Xu, G. Li, J. Liu and G. Chen, *Int. J. Hydrogen Energy*, 2013, 38, 9137.
- 40 P. Sun, S. Du, T. Yang, X. Li, F. Liu, X. Liang, Y. Gao, Y. Sun and G. Lu, *Rsc Adv.*, 2013, 3, 7112.
- 5 41 Y. Zhao, H. Shi, M. Chen and F. Teng, *CrystEngComm*, 2014, 16, 2417.
- 42 R. Dong, L. Zhou, D. Wang and J. Hao, *Sci. Rep.*, 2013, 3.
- 43 Y. Song, H. Zou, Y. Sheng, K. Zheng and H. You, *J. Phys. Chem. C*, 2011, 115, 19463.
- 10 44 S. Li, X. Zhang, Z. Hou, Z. Cheng, P. Ma and J. Lin, *Nanoscale*, 2012, 4, 5619.
- 45 K. Kimpe, T. N. Parac-Vogt, S. Laurent, C. Pierart, L. V. Elst, R. N. Muller and K. Binnemans, *Eur. J. Inorg. Chem.*, 2003, 3021.
- 46 Z. Dou, J. Yu, Y. Cui, Y. Yang, Z. Wang, D. Yang and G. Qian, *J. Am. Chem. Soc.*, 2014, 136, 5527.
- 15 47 R. Cao, D. Sun, Y. Liang, M. Hong, K. Tatsumi and Q. Shi, *Inorg. Chem.*, 2002, 41, 2087.
- 48 M. Arduini, F. Mancin, P. Tecilla and U. Tonellato, *Langmuir*, 2007, 23, 8632.
- 20 49 R. de la Rica, E. Mendoza and H. Matsui, *Small*, 2010, 6, 1753.
- 50 Z. Wang, J. H. Lee and Y. Lu, *Adv. Mater.*, 2008, 20, 3263.
- 51 J. Tang and A. P. Alivisatos, *Nano Lett.*, 2006, 6, 2701.

Graphic Abstract



Straw-sheaf-like terbium-based coordination polymer (CP) architectures have been successfully synthesized through a microwave heating approach and they showed highly sensitive and selective luminescence quenching to Pb²⁺ in aqueous solution.